Journal of Power Sources xxx (xxxx) xxx

Contents lists available at ScienceDirect

Journal of Power Sources

journal homepage: www.elsevier.com/locate/jpowsour

Lithium heterogeneities in cylinder-type Li-ion batteries – fatigue induced by cycling

D. Petz [a], M.J. Mühlbauer [a,b,c], V. Baran [a], M. Frost [d], A. Schökel [e], C. Paulmann [e,f], Y. Chen [d], D. Garcés [a,g], A. Senyshyn [a,*]

[a] Heinz Maier-Leibnitz Zentrum (MLZ), Technische Universität München, Lichtenbergstr. 1, 85748, Garching, Germany
[b] Helmholtz-Institute Ulm for Electrochemical Energy Storage (HIU), P.O. Box 3640, D-76021, Karlsruhe, Germany
[c] Institute for Applied Materials (IAM), Karlsruhe Institute of Technology (KIT), Hermann-von-Helmholtz-Platz 1, D-76344, Eggenstein-Leopoldshafen, Germany
[d] Spallation Neutron Source, Neutron Scattering Division, Oak Ridge National Laboratory, Oak Ridge, TN, 37830, United States
[e] Deutsches Elektronen Synchrotron (DESY), Notkestr. 85, 22607, Hamburg, Germany
[f] Mineralogisch-Petrographisches Institut, Universität Hamburg, Grindelallee 48, 20146, Hamburg, Germany
[g] CNEA-INN, Centro Atómico Constituyentes, San Martin, B1650, KNA, Argentina

HIGHLIGHTS

- *Lithium/SOC distribution was studied in operando using ToF* neutron diffraction.
- Lithium/SOC distribution was probed using ex situ X-ray diffraction radiography.
- Fatigue –driven spatial heterogeneity of lithium distribution is reported.
- SOC heterogeneities at the anode stripe systematically occur due to cell cycling.

ARTICLE INFO

Keywords:
Li-ion batteries
18650
Type
Time-of-flight neutron powder diffraction
Synchrotron radiation
X-ray diffraction radiography

ABSTRACT

Integrity and uniformity are crucial factors for stable, safe, robust and well-predicted operation of Li-ion batteries. The uniformity of lithium distribution in the graphite anode in fully charged state was studied by a combination of spatially-resolved time-of-flight neutron diffraction, powder diffraction using synchrotron radiation and electrochemical measurements. Studies were carried out on a series of NCA|C Li-ion cells of 18650-type with various cycle numbers. Experimentally obtained lithium distribution under in operando and ex situ conditions have been found in fair agreement and revealed a non-uniform character of lithiation in the graphite anode in charged state, where the degree of heterogeneity increases with the number of cycles.

1. Introduction

As the demand of mobile electronic devices is rapidly growing, there is a permanent need in rechargeable batteries with higher energy and power densities at lower cost. Currently, these requirements are best fulfilled by lithium-ion batteries [1,2], which to a large extent explains their rapid spread and popularity. In the case of Li-ion batteries cell performance and lifetime is determined by internal chemical and structural parameters of the cell constituents as well as external parameters like cell design, integration and its operating conditions.

A closed electrochemical systems like Li-ion batteries often require non-destructive methods for their characterization and study in order to avoid changes of material parameters, e.g. the ones caused by oxidation of electrode material, evaporation of electrolyte, etc. For such non-destructive measurements neutron scattering is a well-established tool having numerous advantages [3]: weak interaction with matter resulting in a high penetration depth; ability to localize light elements next to heavy ones due to large variations in scattering cross section; contrast for different isotopes and complementarity of the obtained information to X-ray diffraction; independence of the scattering length from $\sin(\Theta)/\lambda$ due to the interaction with the nuclei, leading to accurate structure factors. Neutron scattering has been utilized for battery research in different applications, e.g. neutron imaging [4–8], reflectometry [9], small-angle scattering [10–12], quasi-elastic neutron scattering [13],

* Corresponding author.
E-mail address: anatoliy.senyshyn@gmail.com (A. Senyshyn).

https://doi.org/10.1016/j.jpowsour.2019.227466
Received 29 July 2019; Received in revised form 31 October 2019; Accepted 14 November 2019

where powder diffraction [6,7,14–38] is the most popular research methodology. Neutron diffraction is often applied to study the crystal structure of either common or potentially new electrode materials under *ex situ* and *in operando* conditions. Monitoring of structural changes correlated to state-of-charge (SOC) give rise to the structural behavior of battery materials at real operating conditions. The majority of diffraction is performed with large volume portions of the cell exposed to the neutron beam assuming homogeneity of the cell. However, some heterogeneities of the current distribution inside real cells were reported [39–43], which may directly be related to non-uniformities in the SOC distribution and, correspondingly, a heterogeneous degradation due to different stress on the electrode particles. For example, Cai et al. [44] found a non-uniform degradation in large format pouch bag cells using time-of-flight neutron diffraction as a local probe. Yu et al. [45] further reported a way for simultaneous monitoring of local temperature, SOC and strain. Recent spatially-resolved monochromatic neutron diffraction studies revealed a heterogeneous distribution of lithium in 18650-type cells in fresh state [46], which further increases upon cell fatigue [47].

The achieved spatial resolution is a parameter of primary interest in a spatially-resolved neutron diffraction experiment (either monochromatic or time-of-flight). Typically an incoming monochromatic neutron beam of 2 mm in width and a radial oscillating collimator with 2 mm horizontal field of view create a square 2×2 mm^2 cross section of the gauge volume in case the detector is set orthogonal to the incoming beam. Using a wavelength of ca. 1.6 Å, which is a compromise between neutron flux, instrumental resolution and sample attenuation, sets the angular range of interest to $26 \pm 5^\circ$ 2θ. This results in a distortion of the squared cross section of the gauge volume to a rhomboid with short and long diagonals equal to ≈2.1 and 8.9 mm. Such coarse spatial resolution may not be optimal for studies of a cell rollover with a 300 μm thick separator-anode-separator-cathode stack. Therefore the reduction of the gauge volume is very important for further studies of the lithium distribution in state-of-the art Li-ion cells having a complex organization of electrodes. With respect to this, spatially-resolved time-of-flight neutron diffraction is a more promising method as it is initially based on a fixed orthogonal geometry of detector and neutron beam, which maintains a square-shaped gauge volume. In the current manuscript, we report the application of time-of-flight spatially-resolved neutron diffraction to study the lithium distribution in cylinder-type Li-ion cells.

2. Experimental

2.1. Electrochemical cycling

A set of 18650-type Li-ion cells (NCA|C, NCR18650B type) with NCA – $LiNi_{0.80}Co_{0.15}Al_{0.05}O_2$ composition was cycled 120, 210 and 400 times at ambient temperature using CCCV (constant current - CC constant voltage - CV) charge at 1.625 A and CC discharge at 6 A. In order to introduce rapid cell fatigue, the cycling currents were set close to the specified maximum of C/2 for charge and 2C for discharge. The voltage window was 2.5–4.2 V, the CV cutoff current was set to 170 mA ≈ C/20 and 15 min time of rest were applied after charging and discharging. Prior to the neutron experiment the cells were reconditioned using slow CCCV charge/discharge with 0.4 A (≈0.12C) current and C/100 CV cutoff, repeated three times ending in fully charged state (SOC = 100%).

2.2. Details of neutron diffraction experiments

An initial structural characterization was performed using high-resolution neutron powder diffraction at the diffractometer SPODI at the Heinz Maier-Leibnitz Zentrum (FRM II, Garching, Germany) [48]. Similar to previously-reported experiments [24], the studied cell was mounted on the sample table of the powder diffractometer and a diffraction pattern over 160 deg. 2θ and 15 deg. ν was collected in ca. 4 h using a wavelength of 1.5482 Å obtained by the (551) reflection of a vertically focused Ge monochromator at 155° take-off angle. There monochromatic beam with a cross-section of 40×20 mm^2 illuminated ca. 70–85% of the entire cell.

Spatially-resolved time-of-flight neutron diffraction studies were performed at the Engineering Materials Diffractometer VULCAN at Spallation Neutron Source (SNS, Oak Ridge, United States) [49]. The experimental setup is very similar to the one reported in Ref. [32], where the major difference is the use of time-of-flight neutron diffraction rather than monochromatic one. Data acquisition in time-of-flight mode enables for a square-shaped cross section of the gauge volume leading to improved spatial resolution, when compared to Refs. [32,46,47]. Sketch and photo of the experimental setup are shown in Fig. 1a–b. Each cell, slowly charged, was mounted on the sample goniometer and its position was aligned using a system of cameras located at ±45° (accuracy better than 100 μm) with respect to the incoming beam. The gauge volume of $2 \times 2 \times 12$ mm^3 was defined using sample slits with 2 mm horizontal opening and a radial oscillating collimator with 2 mm field of view. In order to enhance counting statistics the vertical beam size was set to 12 mm, in agreement with the radial symmetry of the studied cells. Due to the specific neutron spectrum and rather high neutron attenuation the direct observation of the (001) LiC_6: (002) LiC_{12} reflection couple (similar to Refs. [32,46]) has been found non optimal. Therefore, 2nd order reflections, namely (002) LiC_6 and (004) LiC_{12} were monitored in detail. In order to focus on selected range-of-interest and maintain high neutron flux, the measured d-space range was narrowed to 1.6–2.2 Å using the 60 Hz chopper setting with wavelength center at 2.7 Å, although the 20 Hz chopper setting has maintained a larger d-spacing coverage of 0.5–3.4 Å. With a combination of translational and rotational degrees of freedom at the sample positioning stage of VULCAN, a number of different gauge volumes in the center plane of the 18650 cells was irradiated (as sketched in Fig. 1c).

2.3. X-ray diffraction studies

For this purpose the 18650-type cell (belonging to the same batch) was charged to SOC = 100% and disassembled in a glove box. Its electrode sheets were unrolled and separated. The double-coated anode stripe (active material and copper current collector) about 520×65 mm^2 was cut into 5 pieces. Each electrode piece was mounted in an isolated frame consisting of an aluminium housing and X-ray transparent capton windows (Fig. 1d). For the current study a "fresh^{I}" and an "aged" cell (cycled 400 times) were disassembled. The electrode of the "fresh^{I}" cell was studied at P24 at PETRA III synchrotron (DESY, Hamburg, Germany) using 20 keV photon energy, whereas the electrode material from the aged cell was investigated at P02.1 using a higher-energy photon beam (60 keV). The crystal structure of lithiated graphite on copper foil was probed using X-ray diffraction radiography [50] with rastering steps of 5.0 mm and 3.0 mm (x and y) at P24 and 4.0 mm and 3.0 mm (x and y) at P02.1. Sketch and photo of experimental setup are shown in Fig. 1e–f). Synchrotron-based diffraction compared to neutron diffraction has an essentially weaker contrast to light atoms. However, the structural details of lithium intercalated graphites along with extremely high signal to noise ratio and excellent counting statistics after 10–30 s of exposure makes synchrotron diffraction (especially high-energy) well – suited for such studies. At P24 a wavelength of 0.6202 Å was used and a MARCCD165 2D detector was placed at a distance of 99.8 mm from the sample, while at P02.1 a PerkinElmer XRD1621 2D detector was used with much larger sample to detector distance of 2466 mm and 0.20714 Å wavelength. Reduction of the obtained 2D diffraction data was performed using Fit2D software [51] based on the data for Si and LaB_6 reference materials.

3. Results and discussion

The initial discharge capacity of the cells was ca. 3170 mAh, sufficiently lower than the nominal capacity of 3400 mAh, which is attributed to the high charge/discharge current. Cycling to 120, 210 and 400

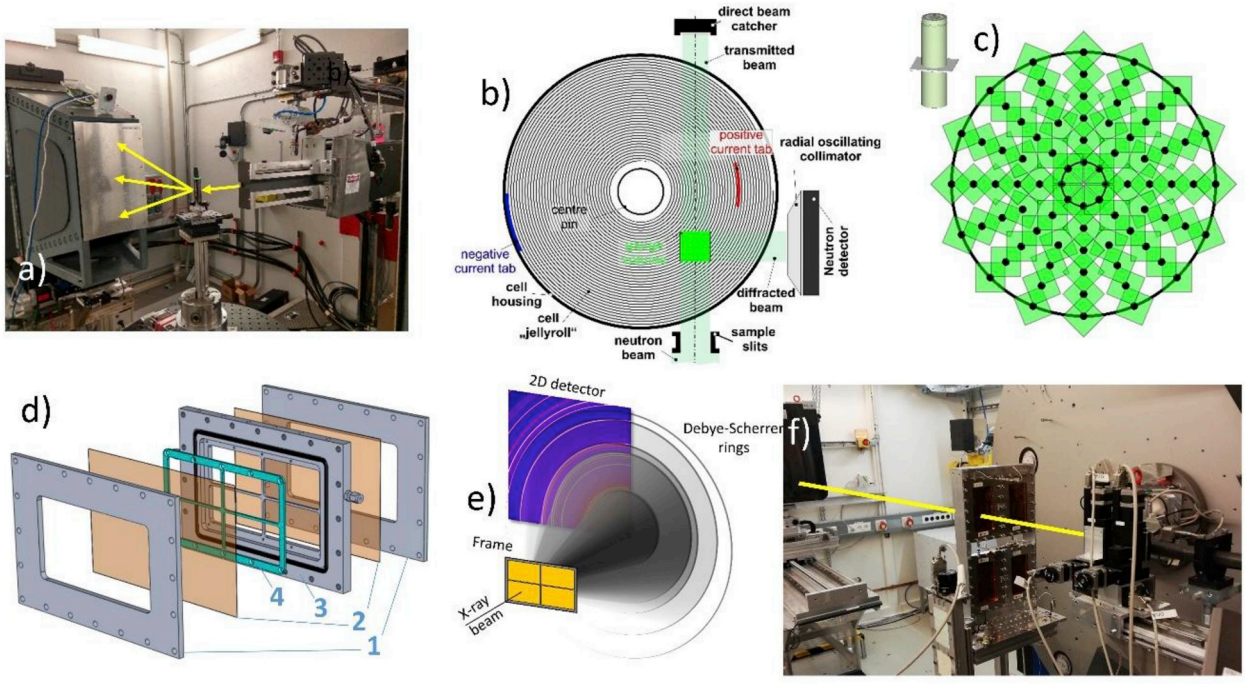

Fig. 1. Photo (a) and sketch (b) of experimental setup utilized in spatially-resolved time-of-flight neutron diffraction experiment and scheme of irradiated gauge volumes on which the diffraction data were collected (c). Exploded view of in situ cell for X-ray diffraction radiography (XRDR) mapping of electrode lithiation (d), where 1 corresponds to front covers, 2 – kapton foils, 3- cell frame and 4 – pressure grid; scheme (e) and photo (f) of experimental setup used in XRDR mapping of lithium in the electrode stripe.

cycles resulted in a reduction of the cell capacity to 2528, 2346 and 1950 mAh, respectively, indicating that at the given cycling conditions a reduced discharge capacity of 80% is reached after approx. 110 cycles already. Using small charge/discharge currents along with low CV cutoff has a positive effect on the relaxation effects and cell uniformity.[1] The evolution of cell capacities of the used cells is depicted in Fig. 2a. The studied cells display sufficiently higher cell capacities when charged with lower current, i.e. 3310, 3161, 3084 and 2982 mAh were obtained for the fresh and cycled cells.

Monochromatic neutron diffraction data were obtained for fresh and cycled NCA|C cylinder-type cells and are plotted in Fig. 2b as a function of interatomic spacing *d*. All experiments were performed at ambient temperature. Similar to previous studies of NMC cell [36], at SOC = 100% the diffraction pattern of a 18650-type cell consists of contributions from the NCA cathode, stage I and stage II lithiated graphites, the Cu and Al current collectors and the steel housing. Analysis of the data reveals a systematic increase of *a* and *c* lattice parameters for the NCA cathode with increasing cycle number, which is also accompanied by the increase of the ratio stage II/stage I of the lithium intercalated graphites. Both effects can be associated with the aging and are driven by a reduction of the lithium concentration in both cathode and anode; corresponding to a loss of movable lithium, similar to the reported losses in 18650-type cells with $LiCoO_2$|C cell chemistry [19]. Following lithium concentrations *x* in the lithiated graphite anode with a general formula Li_xC_6 were determined: 0.851, 0.772, 0.752, 0.701 corresponding to fresh and cycled cells. The obtained behavior of lithium concentration in graphite has been found in good agreement with the observed capacity decrease indicating, that loss of movable lithium is directly related to capacity fade in the studied cells.

Uniformity of the lithium distribution was probed using spatially-resolved time-of-flight neutron powder diffraction. A typical diffraction pattern of a single gauge volume is shown in Fig. 2c, where the excellent resolution of VULCAN at low interatomic spacings (high momentum transfers) made the separation of the desired peaks possible. Based on the diffraction data collected for 80 separate gauge volumes for each cell, the 2D distribution of the lithium concentration x in the lithiated graphite anode Li_xC_6 was obtained (Fig. 3) [46]. Experimental data are plotted by points and a color surface plot indicates the results of a 2D interpolation. Besides several distinct and well-isolated regions exhibiting lower lithiation, the lithium distribution in the studied fresh cell (Fig. 3a) has been found quasi-uniform within the standard deviations. Regions with essentially lower lithium concentration are attributed to places with missing electrode coating, e.g. at the beginning/end of the electrode stripe or at the place of current tab. In general a good agreement of the obtained lithium distribution for the fresh cell (Fig. 3) and previously reported results using monochromatic neutrons (cell 3 in Ref. [46]) is observed.

One can define several statistical parameters to characterize the observed 2D distributions, for example a mean value and its standard deviation having a meaning of average lithium concentration $<x_{Li}>$ and its deviation from constant, median of the distribution and the plateau value x_p. As it can be seen from Fig. 3, the cell fatigue affects the lithium concentration in the graphite anode of fully charged aged cells. With increasing number of cycles all three integral characteristics are reduced, in agreement with above-mentioned monochromatic neutron diffraction studies. However, spatially-resolved diffraction shows a non-uniform character of cell fatigue, similar to $LiCoO_2$|C high-energy cells [47]. This aging effect is better illustrated by 2D distribution of lithium concentrations with subtracted x_p, presented in Fig. 3 (last row), where the surface of light area indicates a plateau region. The region of constant lithium concentration has been found gradually decreasing with cell fatigue, where reduction of its surface indicates the development of non-uniformities. Furthermore, the remaining light-yellow-red regions have been found dominantly present in the outer region of the cell corresponding to systematically higher lithiation (similar to the observations from Ref. [47]). This points to the development of

[1] Therefore, even larger cell non-uniformities have to be expected during the application of higher currents or a premature cutoff during the CV – phase.

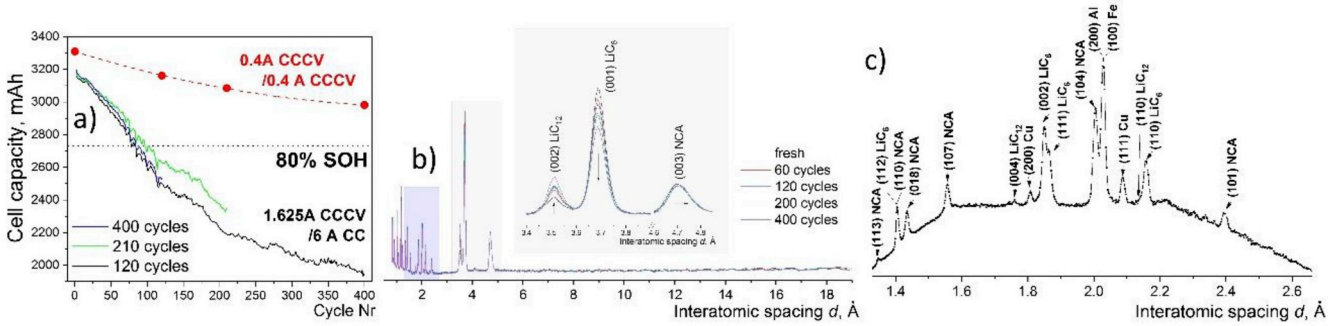

Fig. 2. Evolution of cell capacities vs. cycle number and subsequent slow charge (a); section of high-resolution monochromatic neutron powder diffraction data (intensity vs. interatomic spacing d) from differently cycled/aged cells (b); example of experimental time-of-flight diffraction pattern collected for fresh cell (c).

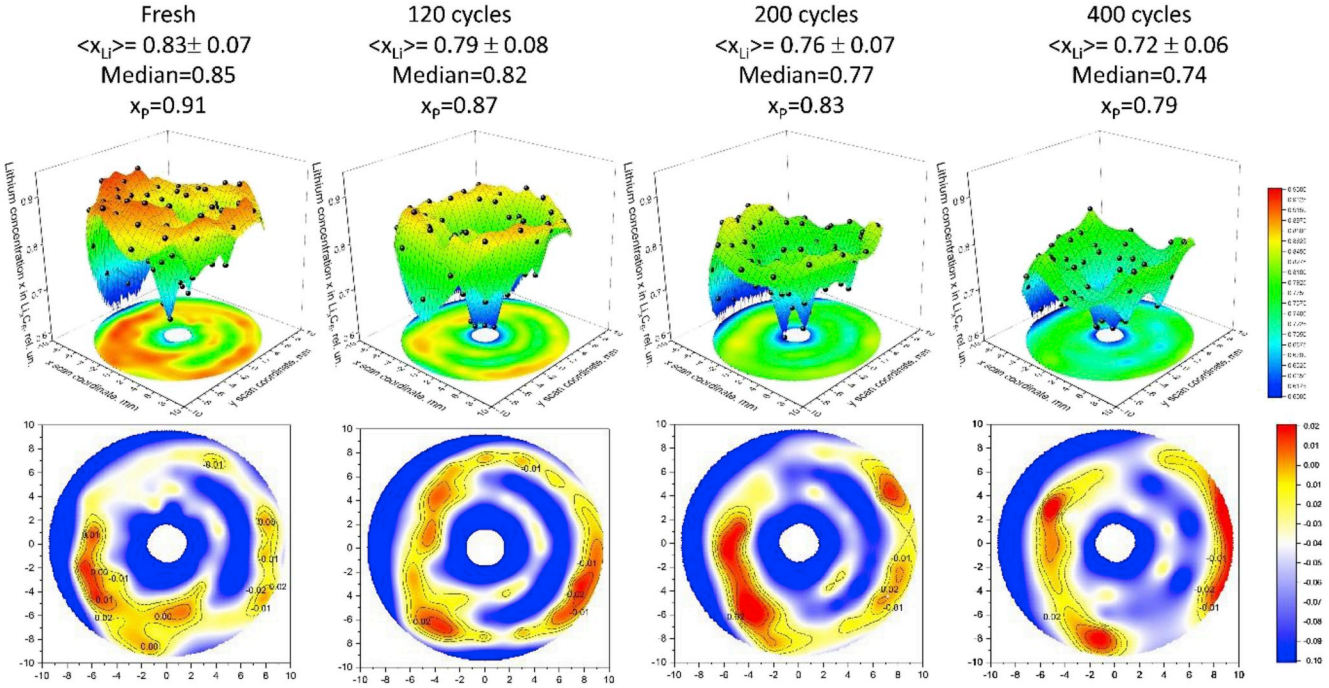

Fig. 3. Experimental lithium distribution vs. cycle number for differently cycled cylinder-type Li-ion batteries as derived from time-of-flight neutron diffraction. (upper row of text) integral characteristics of lithium distribution; in-plane lithium distribution (middle row) and deviations of lithium distribution from plateau value xp (bottom row).

heterogeneities of Li concentration in the graphite anode driven by cell fatigue. However, despite the higher spatial resolutions achieved by time-of-flight neutron diffraction, no sufficient differences to previously reported Li-distribution in similar cells (cell 3 [46]) have been noticed, showing that the 2×2 mm^2 horizontal cross-section of the gauge volume is not sufficient to resolve more details. Lithium distribution may display smaller non-uniformities, i.e. their accurate characterization requires even better spatial resolution hardly accessible by spatially-resolved neutron diffraction. For the measurements at VULCAN the most optimal configuration was applied, where a further reduction of the gauge volume is directly proportional to a reduction of neutron flux on the sample or active sample amount (participating in scattering process). Correspondingly, low counting statistics would then lead to impractically long exposure times.

Among different options available to study the heterogeneity of lithium distribution in cylinder-type cells at higher spatial resolution, the most straightforward one is based on a powder diffraction study of the separate electrodes. Negative electrodes were extracted from "fresh^{I}" and "aged" cell (cycled 400 times) and studied using XRDR technique, where diffraction data are collected on a dense grid of scanned points necessary to obtain the 2D spread of chosen structural properties. Typical diffraction datasets collected at P24 and P02.1 are shown in Fig. 4a–b. From these the x in Li_xC_6 of the studied anodes was obtained using the (001) LiC_6/(002) LiC_{12} reflection ratio, values of structure factors, molar masses and densities (for details please refer to Ref. [46]). The distribution of lithium concentration x over the complete electrode stripe is presented in Fig. 4c, where the lithium concentration is plotted as a false color map (according to the legend) and graphs on the top and right correspond to the averaged values along the anode stripe. At all studied points lithium concentrations $x > 0.5$ in Li_xC_6 have been observed. The experimentally obtained lithium distribution has been found quite heterogeneous, which can to some extent be related to the cell design as the lithium distribution in the graphite anode is largely affected by the coating of the counter electrode (cathode). Besides the current tab around its middle, the cathode stripe is typically shorter in length (and in width) than the corresponding anode and starting/ending positions of its coating can differ on both sides. Taking into account that structural information from both sides of the graphite anode is present in the diffraction data collected in transmission mode this is a crucial factor. Furthermore a lack of counter electrode coating may form

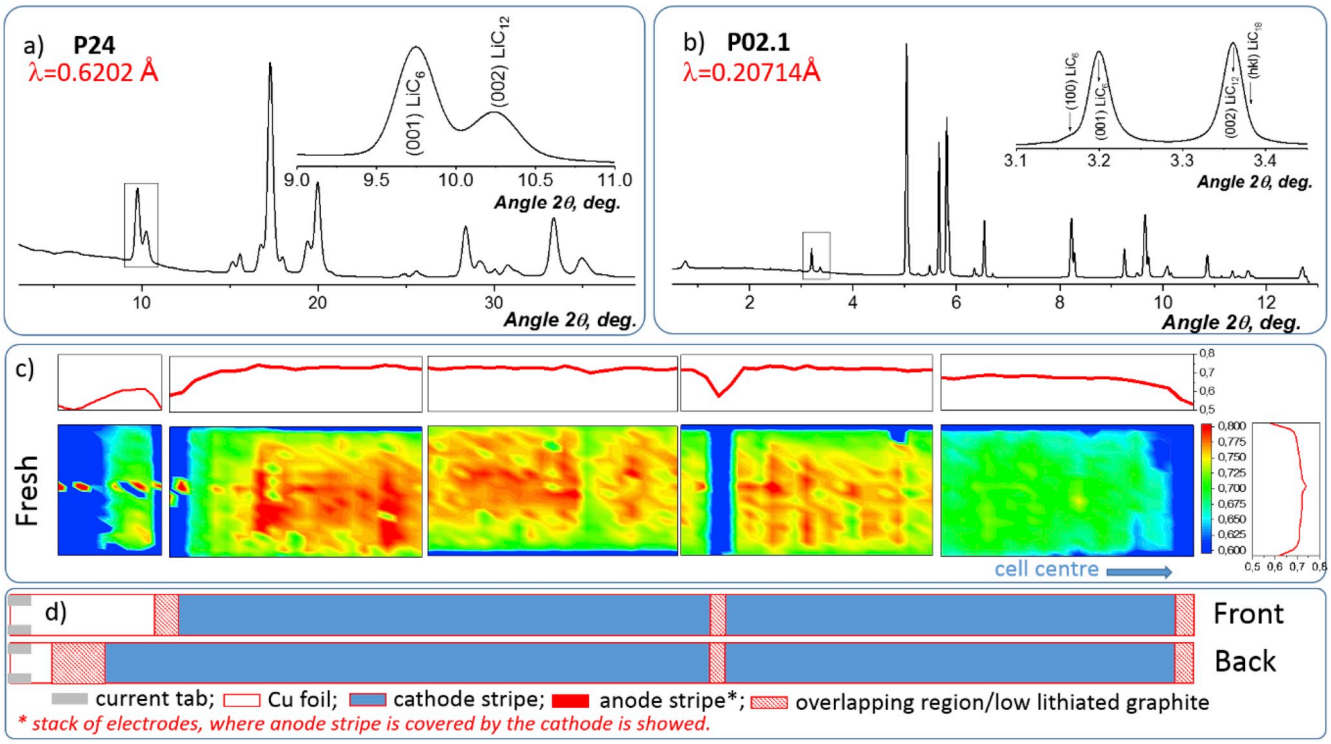

Fig. 4. Typical diffraction data collected at P24 (a) and P02.1 (b) diffractometers; experimentally observed 2D distribution of lithium in fresh cell and averages over long and short edges of the electrode stripe (e); scheme of electrode arrangement in studied cells (f).

regions with geometrically limited lithium exchange [46], which may further result in low lithiation.

A sketch of the electrode coating is presented in Fig. 4d, where four distinct regions displaying areas with lower lithium concentration can be identified and traced back in the experimental lithium concentration map displayed in Fig. 4c. Neglecting the regions with geometrically limited lithium diffusion, the Li distribution in the graphite anode of the "fresh^{I}" cell can be concluded to be uniform in a first approximation. However, detailed analysis of average profiles along the width and length of the anode stripe revealed a weak, but systematic, reduction of lithium concentrations towards cell center along the electrode stripe and towards the cell top and bottom, when considering the electrode width. A similar behavior of the lithium concentrations along the length of an electrode stripe and perpendicular to it have been already observed in Refs. [46,47] and was attributed to possible non-uniformities of current and electrolyte distribution.

Studies of the "fatigued" cell[2] using high – energy synchrotron radiation resulted in a very similar behavior (Fig. 5). One can clearly resolve three regions with lower lithium concentrations in the graphite anode associated with the missing cathode coating. In agreement with spatially-resolved neutron diffraction and residual cell capacity resulting from electrochemical measurements a sufficiently lower overall lithium concentration (x in Li_xC_6) has been found in the aged cell (x = 0.645 in "aged" cell vs. x = 0.709 in "fresh^{I}" cell), which is corresponding to a loss of mobile lithium. From the detailed analysis of lithiation profiles obtained along the length of the anode stripe of the fatigued cell, one can also notice a reducing gradient of lithium concentration towards cell center. The lithiation profile along the width of the anode stripe (corresponding to the height of cylinder cell) has been found deviating from the constant at top and bottom regions. Comparing the obtained profiles to the results of the "fresh^{I}" cell unambiguously reveals an increased heterogeneity of the lithium distribution upon cell fatigue at the top and bottom edges of the electrode.

The improved peak resolution of the P02.1 setup allowed to reveal the presence of a tail at the (002) reflection of stage II (LiC_{12}) at higher 2θ angles (previously mentioned in Ref. [50]), which was attributed to the presence of lithiated graphite with the lithiation grade x < 0.5 in Li_xC_6, i.e. $LiC_{x>12}$. A profile decomposition with subsequent 2D mapping of the ratio of the tail of (hkl) $LiC_{x>12}$ reflection intensity to (002) LiC_{12} reflection intensity clearly yielded to a strong presence of low-lithiated graphite $LiC_{x>12}$ at places previously identified as regions with lower lithium concentration due to missing cathode coating (Fig. 5, bottom row). The intensity ratio for (hkl) $LiC_{x>12}$/(002) LiC_{12} can be used as a sensitive indicator for the presence of lower lithiated graphites, which at SOC = 100% is often considered to be a factor supplementing the lithium plating. However, careful analysis of the intensity distribution at the peak positions corresponding to metallic lithium did not reveal the presence of a lithium signal with measurable confidence.

4. Conclusions

In summary, the uniformity of the lithium distribution inside the graphite anode in fully charged state of a series of differently cycled Li-ion cells was studied using spatially-resolved time-of-flight neutron powder diffraction under *in operando* conditions. The studied cells were cycled with a charging protocol close to the maximum allowed by the cell manufacturer, which resulted in a rapid cell fatigue. The analysis of the lithium distribution profiles revealed a systematic reduction of the lithium concentration with extensive cell cycling, which is supplemented by larger deviations from a constant (plateau-like) behavior. Supplementary (*quasi ex situ*) characterization of lithium concentrations of disassembled anode stripes using XRDR resulted in a gradient of the lithium concentration along the length and width of the unrolled electrode stripe. Cell cycling caused gradients to increase, pointing the non-uniform character of the fatigue. Using three different techniques (high-resolution monochromatic neutron powder diffraction, spatially-

[2] The last piece of the graphite anode remained not studied due to time limitations.

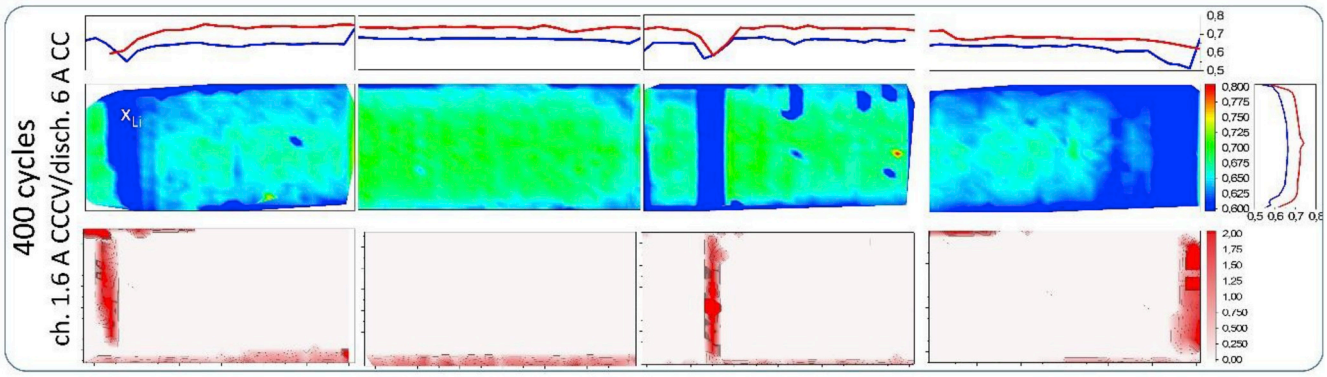

Fig. 5. Experimentally observed 2D distribution of lithium in fatigued cell; corresponding averages in x and y directions of the electrode stripe (fresh^{I} – red line, fatigued – blue line) and intensity ratio of anomalous $LiC_{x>12}$ (hkl) to LiC_{12} (002) reflections (bottom row). (For interpretation of the references to color in this figure legend, the reader is referred to the Web version of this article.)

resolved time-of-flight neutron powder diffraction and diffraction using synchrotron radiation) at four separate instruments yielded clear and consistent results supplementing each other and showing a development of non-uniformities during cell fatigue.

We believe this effect to be crucial for the cell performance, safety and lifetime and attribute it to current and electrolyte distribution as well as its dynamics and evolution *vs.* cell cycling. As it has recently been shown the current distribution can be quantified fairly well by combining a multi-tab approach with finite element cell modeling [52]. The role of the electrolyte distribution still remains quite unclear and an experimental methodology capable to quantify the electrolyte distribution under *in operando* conditions is highly desired for deeper understanding of the processes supplementing the cell fatigue in real Li-ion cells. For example, application of neutron-based imaging for qualitative studies of electrolyte distribution has been reported in literature, but its application for quantitative studies is not trivial. Thermography [53] or advanced spectroscopy techniques [54] display very promising results in non-destructive spatial quantification of electrolyte for lab based cells, which can potentially be extended for commercial standards. A possible approach to minimize the observed heterogeneities would be the control of tortuosity of porous particles along the electrode stripe [55], i.e. having a certain porosity gradient from inner to outer end of the electrode stripe.

It requires a development of research methodologies, where further improvement of spatial resolution in spatially-resolved diffraction from electrochemical storage systems or *ex situ* XRDR analysis of harvested electrodes is highly important to reveal smaller non-uniformities having their impact on the battery safety, stability and performance. For example recently crystallographic heterogeneities within Si/graphite anode reported with unprecedented spatial resolution of 1 μm [56] making it suitable for studies of lithiation processes in particles and engineered surfaces and composites [57,58]. Bright perspectives and an overall relevance of diffraction techniques using focused beams of high-energy photons or thermal neutrons for studies of non-uniformities in energy storage systems can be unambiguously identified.

Declaration of competing interest

The authors declare that they have no known competing financial interests or personal relationships that could have appeared to influence the work reported in this paper.

Acknowledgment

This work was in part supported by Technische Universität München, Karlsruhe Institute of Technology and PETRA III synchrotron. Technical assistance and help of Mr. J. Pfanzelt is gratefully acknowledged. The authors also acknowledge DESY (Hamburg, Germany), a member of the Helmholtz Association HGF, SNS and MLZ for the granted access to their experimental facilities. Studies using synchrotron radiation were carried out at PETRA III synchrotron using beamline P02.1 and P24. Time-of-flight neutron diffraction experiments were carried out at the Spallation Neutron Source (SNS), which is the U.S. Department of Energy (DOE) user facility at the Oak Ridge National Laboratory, sponsored by the Scientific User Facilities Division, Office of Basic Energy Sciences.

References

[1] J.M. Tarascon, M. Armand, Nature 414 (2001) 359–367.
[2] J.M. Tarascon, Phil. Trans. R. Soc. A 368 (2010) 3227–3241.
[3] P.P.R.M.L. Harks, F.M. Mulder, P.H.L. Notten, J. Power Sources 288 (2015) 92–105.
[4] K. Kino, M. Yonemura, Y. Kiyanagi, Y. Ishikawa, J.D. Parker, T. Tanimori, T. Kamiyama, Phys. Proc. 69 (2015) 612–618.
[5] L.G. Butler, B. Schillinger, K. Ham, T.A. Dobbins, P. Liu, J.J. Vajo, Nucl. Instrum. Methods A 651 (2011) 320–328.
[6] L.G. Butler, E.H. Lehmann, B. Schillinger, in: 7th International Topical Meeting on Neutron Radiography (Itmnr-7) 43, 2013, pp. 331–336.
[7] H. Zhou, K. An, S. Allu, S. Pannala, J.L. Li, H.Z. Bilheux, S.K. Martha, J. Nanda, ACS Energy Lett. 1 (2016) 981–986.
[8] J.B. Siegel, X.F. Lin, A.G. Stefanopoulou, D.S. Hussey, D.L. Jacobson, D. Gorsich, J. Electrochem. Soc. 158 (2011) A523–A529.
[9] J.E. Owejan, J.P. Owejan, S.C. DeCaluwe, J.A. Dura, Chem. Mater. 24 (2012) 2133–2140.
[10] C.A. Bridges, X.G. Sun, J.K. Zhao, M.P. Paranthaman, S. Dai, J. Phys. Chem. C 116 (2012) 7701–7711.
[11] S.M. Mamun, M. Herstedt, K. Oikawa, T. Gustafsson, T. Otomo, M. Furusaka, T. Kamiyama, H. Sakaebe, K. Edstrom, Appl. Phys. Mater. 74 (2002) S1028–S1030.
[12] S. Seidlmayer, J. Hattendorff, I. Buchberger, L. Karge, H.A. Gasteiger, R. Gilles, J. Electrochem. Soc. 162 (2015) A3116–A3125.
[13] S.K. Fullerton-Shirey, J.K. Maranas, Macromolecules 42 (2009) 2142–2156.
[14] O. Bergstrom, A.M. Andersson, K. Edstrom, T. Gustafsson, J. Appl. Crystallogr. 31 (1998) 823–825.
[15] F. Rosciano, M. Holzapfel, W. Scheifele, P. Novak, J. Appl. Crystallogr. 41 (2008) 690–694.
[16] N. Paul, J. Wandt, S. Seidlmayer, S. Schebesta, M.J. Muehlbauer, O. Dolotko, H. A. Gasteiger, R. Gilles, J. Power Sources 345 (2017) 85–96.
[17] N. Sharma, V.K. Peterson, Electrochim. Acta 101 (2013) 79–85.
[18] M. Roberts, J.J. Biendicho, S. Hull, P. Beran, T. Gustafsson, G. Svensson, K. Edstrom, J. Power Sources 226 (2013) 249–255.
[19] O. Dolotko, A. Senyshyn, M.J. Muhlbauer, K. Nikolowski, F. Scheiba, H. Ehrenberg, J. Electrochem. Soc. 159 (2012) A2082–A2088.
[20] A. Senyshyn, M.J. Muhlbauer, O. Dolotko, M. Hofmann, H. Ehrenberg, Sci. Rep 5 (2015).
[21] M.A. Rodriguez, M.H. Van Benthem, D. Ingersoll, S.C. Vogel, H.M. Reiche, Powder Diffr. 25 (2010) 143–148.
[22] J. Wilhelm, S. Seidlmayer, S. Erhard, M. Hofmann, R. Gilles, A. Jossen, J. Electrochem. Soc. 165 (2018) A1846–A1856.
[23] N. Sharma, V.K. Peterson, J. Solid State Electrochem. 16 (2012) 1849–1856.
[24] A. Senyshyn, M.J. Muhlbauer, K. Nikolowski, T. Pirling, H. Ehrenberg, J. Power Sources 203 (2012) 126–129.
[25] H.D. Liu, C.R. Fell, K. An, L. Cai, Y.S. Meng, J. Power Sources 240 (2013) 772–778.
[26] A. Senyshyn, O. Dolotko, M.J. Muhlbauer, K. Nikolowski, H. Fuess, H. Ehrenberg, J. Electrochem. Soc. 160 (2013) A3198–A3205.
[27] B.H. Song, G.M. Veith, J. Park, M. Yoon, P.S. Whitfield, M.J. Kirkham, J. Liu, A. Huq, Chem. Mater. 31 (2019) 124–134.

[28] I.A. Bobrikov, N.Y. Samoylova, D.A. Balagurov, O.Y. Ivanshina, O.A. Drozhzhin, A. M. Balagurov, Russ. J. Electrochem. 53 (2017) 178–186.
[29] J.J. Biendicho, M. Roberts, C. Offer, D. Noreus, E. Widenkvist, R.I. Smith, G. Svensson, K. Edstrom, S.T. Norberg, S.G. Eriksson, S. Hull, J. Power Sources 248 (2014) 900–904.
[30] N. Sharma, V.K. Peterson, J. Power Sources 244 (2013) 695–701.
[31] M.A. Rodriguez, D. Ingersoll, S.C. Vogel, D.J. Williams, Electrochem. Solid State 7 (2004) A8–A10.
[32] A. Senyshyn, M.J. Muhlbauer, O. Dolotko, M. Hofmann, T. Pirling, H. Ehrenberg, J. Power Sources 245 (2014) 678–683.
[33] N. Sharma, V.K. Peterson, M.M. Elcombe, M. Avdeev, A.J. Studer, N. Blagojevic, R. Yusoff, N. Kamarulzaman, J. Power Sources 195 (2010) 8258–8266.
[34] H. Berg, H. Rundlov, J.O. Thomas, Solid State Ion. 144 (2001) 65–69.
[35] N. Sharma, M.V. Reddy, G.D. Du, S. Adams, B.V.R. Chowdari, Z.P. Guo, V. K. Peterson, J. Phys. Chem. C 115 (2011) 21473–21480.
[36] O. Dolotko, A. Senyshyn, M.J. Muhlbauer, K. Nikolowski, H. Ehrenberg, J. Power Sources 255 (2014) 197–203.
[37] S.K. Jha, H. Charalambous, J.S. Okasinski, T. Tsakalakos, J. Mater. Sci. 54 (2019) 2358–2370.
[38] X.L. Wang, K. An, L. Cai, Z.L. Feng, S.E. Nagler, C. Daniel, K.J. Rhodes, A.D. Stoica, H.D. Skorpenske, C.D. Liang, W. Zhang, J. Kim, Y. Qi, S.J. Harris, Sci. Rep 2 (2012).
[39] G.S. Zhang, C.E. Shaffer, C.Y. Wang, C.D. Rahn, J. Electrochem. Soc. 160 (2013) A610–A615.
[40] P. Taheri, A. Mansouri, B. Schweitzer, M. Yazdanpour, M. Bahrami, J. Electrochem. Soc. 160 (2013) A1731–A1740.
[41] G.S. Zhang, C.E. Shaffer, C.Y. Wang, C.D. Rahna, J. Electrochem. Soc. 160 (2013) A2299–A2305.
[42] S.J. Harris, A. Timmons, D.R. Baker, C. Monroe, Chem. Phys. Lett. 485 (2010) 265–274.
[43] P.R. Shearing, L.E. Howard, P.S. Jorgensen, N.P. Brandon, S.J. Harris, Electrochem. Commun. 12 (2010) 374–377.
[44] L. Cai, K. An, Z.L. Feng, C.D. Liang, S.J. Harris, J. Power Sources 236 (2013) 163–168.
[45] X. Yu, Z. Feng, Y. Ren, D. Henn, Z. Wu, K. An, B. Wu, C. Fau, C. Li, S.J. Harris, J. Electrochem. Soc. 165 (2018) A1578–A1585.
[46] A. Senyshyn, M.J. Muhlbauer, O. Dolotko, M. Hofmann, H. Ehrenberg, Sci. Rep. 5 (2015) 18380.
[47] M.J. Muhlbauer, O. Dolotko, M. Hofmann, H. Ehrenberg, A. Senyshyn, J. Power Sources 348 (2017) 145–149.
[48] M. Hoelzel, A. Senyshyn, N. Juenke, H. Boysen, W. Schmahl, H. Fuess, Nuclear instruments and methods in physics research section A: accelerators, spectrometers, detectors and associated equipment 667 (2012) 32–37.
[49] X.L. Wang, T.M. Holden, G.Q. Rennich, A.D. Stoica, P.K. Liaw, H. Choo, C. R. Hubbard, Phys. B Condens. Matter 385 (2006) 673–675.
[50] M.J. Mühlbauer, A. Schökel, M. Etter, V. Baran, A. Senyshyn, J. Power Sources 403 (2018) 49–55.
[51] A.P. Hammersley, S.O. Svensson, M. Hanfland, A.N. Fitch, D. Hausermann, High Press. Res. 14 (1996) 235–248.
[52] P.J. Osswald, S.V. Erhard, A. Noel, P. Keil, F.M. Kindermann, H. Hoster, A. Jossen, J. Power Sources 314 (2016) 93–101.
[53] J.B. Robinson, E. Engebretsen, D.P. Finegan, J. Darr, G. Hinds, P.R. Shearing, D.J. L. Brett, ECS Electrochem. Lett. 4 (2015) A106–A109.
[54] Y.P. Stenzel, F. Horsthemke, M. Winter, S. Nowak, Separations 6 (2019) 26.
[55] S. Müller, J. Eller, M. Ebner, C. Burns, J. Dahn, V. Wood, J. Electrochem. Soc. 165 (2018) A339–A344.
[56] D.P. Finegan, A. Vamvakeros, L. Cao, C. Tan, T.M.M. Heenan, S.R. Daemi, S.D. M. Jacques, A.M. Beale, M. Di Michiel, K. Smith, D.J.L. Brett, P.R. Shearing, C. Ban, Nano Lett. 19 (2019) 3811–3820.
[57] Y. An, H. Fei, G. Zeng, L. Ci, S. Xiong, J. Feng, Y. Qian, ACS Nano 12 (2018) 4993–5002.
[58] J. Feng, Z. Zhang, L. Ci, W. Zhai, Q. Ai, S. Xiong, J. Power Sources 287 (2015) 177–183.